Journal of Applied Polymer Science

Microstructural, wetting, and dielectric properties of plasma polymerized polypyrrole thin films

Hari Krishna Koduru,[1] Lucia Marino,[1] Janardhanam Vallivedu,[2] Chel-Jong Choi,[2] Nicola Scaramuzza[1,3]

[1]Dipartimento Di Fisica, Università Degli Studi Della Calabria, via P. Bucci, 33B – 87036, Cubo, Rende (CS), Italy

[2]School of Semiconductor and Chemical Engineering, Semiconductor Physics Research Center (SPRC), Chonbuk National University, Jeonju, 561-756, Republic of Korea

[3]CNISM – Unità Di Ricerca Di Cosenza C/O Dipartimento Di Fisica, Università Degli Studi Della Calabria, via P. Bucci, 31C – 87036, Cubo, Rende (CS), Italy

Correspondence to: H. K. Koduru (E-mail: koduruharika@gmail.com)

ABSTRACT: Polypyrrole (PPy) thin films were synthesized by plasma polymerization technique and investigated the influence of discharge power on microstructural, optical, surface wettability, and dielectric properties of grown films. As deposited PPy films were characterized by X-ray diffraction (XRD), Fourier transform Infrared spectroscopy (FTIR), Atomic force microscopy, UV-VIS spectroscopy and dielectric spectroscopy. The broad XRD peak present at $2\theta = 23.5^{\circ}$ revealed the amorphous nature of grown PPy films. The FTIR spectra displayed characteristic peaks in the wavenumbers regions 3300–3400 cm^{-1} and 1635–1700 cm^{-1} and respective peaks intensities decreased slightly as a function of discharge powers. Significant modifications in surface morphology of the films were observed as a function of discharge powers and PPy films synthesized at higher discharge power of 50 W demonstrated characteristic surface morphology composed of characteristic vertical cone shaped clusters provided with rms roughness of 3.42 nm. The UV-VIS absorption spectra evidenced that the optical density values varied as a function of discharge power. The evaluated band gap energies decreased with an increase of discharge power and found to be 2.53 eV for PPy films prepared at higher discharge power of 50 W. The surface wettability studies evidenced that as prepared PPy films were found to be hydrophilic in nature. The dielectric measurements were carried out for "ITO/polymer/ITO" structures in the frequency range 10 mHz to 100 kHz. As evidenced from dielectric spectroscopic measurements, PPy films synthesized at 50 W were demonstrated conductivity value of 6.0×10^{-12} S/m.
 J. Appl. Polym. Sci. **2016**, *133*, 43982.

KEYWORDS: conducting polymers; dielectric properties; films; hydrophilic polymers; optical properties

Received 9 March 2016; accepted 29 May 2016

DOI: 10.1002/app.43982

INTRODUCTION

In recent years, considerable interest has been shown in the fabrication of polymer materials in thin film configuration for wide range of applications from insulators to flexible electronic device components.[1–3] Accordingly, π–conjugated organic polymers have received much attention in both academic and industrial communities in view of their unique combination of properties leading to various promising applications such as sensors, anticorrosion coatings, supercapacitors and batteries, drug delivery, and artificial muscles.[4–11] Among the electroconductive polymers, polypyrrole (PPy) is one of the promising conducting polymer owing to its unique properties like flexibility, good stability, able to tailor made for specific uses and better resistant to chemical attack, and easy film forming property.[12–14] Specifically, PPy thin films can be employed as sensor applications, microactuators, solid electrolytic capacitor, functional membranes, and so forth.[15–18] The performance of PPy thin films, for aforementioned applications, predominantly depends on terms of their quality and structural surface morphological properties. However, the quality and microstructural properties of polymer films mostly depend on type of deposition technique and respective film processing parameters. Thus, currently growing interest has concentrated on preparation of conducting polymer thin films with controlled microstructures using different thin film deposition techniques. In this direction, researchers have employed various deposition methods to prepare conducting polymer thin films in view of spectrum of applications.[19–27]

In among various deposition methods plasma polymerization is a unique and promising technique to prepare quality, pinhole

free & well adherent conducting organic films on a variety of substrates.[28–31] It is worth to mention that, the microstructural properties of plasma polymerized polymer films can be tailored by controlling the growth conditions, such as the deposition time and discharge power. It refers to the deposition of polymer films through plasma dissociation, in which plasma discharge energizes and dissociates the monomer molecules into neutral particles and reactant fragments in the form of electrons, ions, and free radicals. The product of recombination of these fragments on over the surface of substrates is a highly branched and cross linked by three-dimensional network of a plasma polymer. It evokes that, plasma polymerized polymers are expected to be essentially different in microstructural and chemical properties from conventional ones, even if the same monomer is utilized for both plasma and conventional polymerizations.[32,33]

In the present study, DC-glow discharge plasma polymerization technique is employed to synthesize Polypyrrole thin films on ITO coated glass substrates. The as deposited films are characterized by X-ray diffraction (XRD), (FTIR), atomic force microscopy (AFM), UV-VIS spectroscopy, surface wettability studies, and electrochemical impedance spectroscopy (EIS) to understand the influence of discharge power on microstructural, surface wettability, optical, and dielectric properties of grown PPy films. The resultant microstructural and dielectric properties of deposited films are interpreted in terms of film growth conditions. In parallel Havriliak-Negami (H-N) equation is adapted to fit the dielectric spectroscopy (DS) data and to understand the frequency dependency of dielectric parameters such as dielectric strength, relaxation time, and conductivity values.

EXPERIMENTAL

Plasma polymerization process was carried out in a cylindrical shaped plasma discharge chamber (5 cm diameter and 20 cm length), which was coupled to a pyrrole monomer container through standard manifold with flux adjusted by a vacuum cock and needle valve. The discharge chamber consists of anode (Rogowski electrode) and hollow cylindrical cathode (negative Rogowski shape) and the diameter of the cathode is twice the diameter of anode, which were separated at a distance of 10 cm. All film depositions were carried out on ITO coated glass substrates by introducing them at exit of the cathode in downstream plasma. Pyrrole monomer was purchased from Sigma-Aldrich (98%) (distilled before to utilize) and monomer vapors were allowed directly into plasma discharge chamber at a constant flow rate of 0.0225 mL/min for 5 min.[34] The DC source was connected across the two electrodes for the generation of plasma in the chamber and plasma discharge was initiated in argon atmosphere. During film deposition, the base pressure was approximately 1×10^{-3} Torr and the working pressure was 1×10^{-1} Torr. Films were deposited at constant deposition time of 5 min and by varying the discharge powers in the range of 10–50 W. As prepared films were observed to be light brown in color and the measured film thicknesses (Stylus profilometer-Veeco dektak 8) were in the range of 250–295 nm. The XRD data was recorded by Bruker AXS, D8 advance X-ray diffractometer with step width 0.05° and step time of 1.25 s using CuK-alpha radiation ($\lambda = 1.5406$ Å). FTIR spectroscopy measurements were measured in the wavenumber range 400–4000 cm^{-1} using Spectrum One Fourier transform Infrared spectroscopy (FTIR) Perkin Elmer spectrometer in normal transmission mode and confirmed the polymerization of pyrrole monomer by the presence of vibrational modes in respective FTIR spectra. FTIR experiments were performed in dynamic nitrogen atmosphere by averaging 10 scans per sample, keeping an optical resolution of 5 cm^{-1} for all the spectra. The UV-VIS absorption spectra of deposited PPy films were recorded by Cary-5E Varian spectrophotometer. AFM images were acquired with a Nano Focus (MOD-1M Plus and Tip size of 10 nm) in non-contact mode and respective images were analyzed by WS × M 5.0 and Develop 5.0 software for data acquisition and image processing, respectively. Contact angle measurements were carried out in static method using optical contact angle meter (KSV Instruments Ltd., Model: CAM 200). In this process, a sessile water drop was provided over the surface of grown films and captured images of water drops at time intervals of 5 s and the respective data was fitted with CAM 200 optical contact angle software to estimate average contact angles for different frames. Impedance spectroscopy measurements were performed using an EG&G 273A galvanostat-potentiostat/impedentiometer controlled by the impedance software M398 in order to acquire the real and imaginary parts of impedance in the frequency range 10 mHz–100 kHz with a maximum applied voltage of 1.4 V (RMS). The obtained results were fitted with Mathematica curve fitting tool using a self-made software first tested on previously published data and analyzed with commercial software widely used. The use of the self-made software allows us to control, optimally several parameters, which is not possible with the commercial software. The values obtained by means of the fit, allows us to evaluate corresponding dielectric properties such as dielectric strength and conductivity values for the grown films.

RESULTS AND DISCUSSION

Polypyrrole thin films obtained by DC-glow discharge plasma polymerization technique are observed to be quite stable and well adherent to the substrates. The structure of Polypyrrole contains an alternating single and double bond. The single (sigma) bond has electrons localized between the two atoms, but the double (pi) bond has the electrons in lobes above and below the sigma bond (as indicated in Figure 1). Figure 2 represents, FTIR spectra of PPy films polymerized at various discharge powers in the range 10–50 W. FTIR spectra displayed broad vibrational band at 3300–3400 cm^{-1}, which is attributed to sp^3 C—H stretching together with N—H stretching. The presence of other characteristic peak at 1635–1700 cm^{-1} is corresponding to C═N and N—H bending. The intensities of both characteristics peaks (present at 3300–3400 cm^{-1} and 1635–1700 cm^{-1}) are decreased slightly as a function of glow powers. This could be due to decrease in rate of polymerization process and unwanted reactions between energetic of ions, and radicals, which are generated in the collision processes at higher glow powers. In plane vibration and breathing of the pyrrole rings

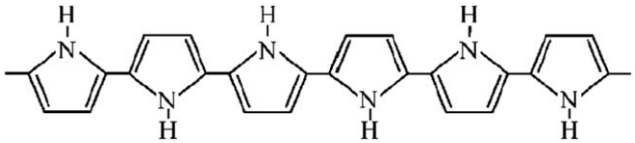

Figure 1. Chemical structure of PPy.

are observed by the bands at 1437, 1381, and 732 cm^{-1}. As a function of discharge power, changes in band intensities of peaks in the wavenumber range 500–1500 cm^{-1} indicates modifications in chemical structure of PPy. In this wavenumber region, the decrease in intensity of respective bands indicate modifications in C—H out of plane of bending, in plane of vibration, C—C stretch and C—N stretch.[35–37] The decrease in intensities of respective bands indicates decrease of ring breathing and increase of stability of pyrrole ring as a function of discharge powers. The presence of prominent bands in finger print region matched with previously reported results for plasma polymerized films.[38–42] One of the disadvantage in plasma assisted polymerization process is the loss of the monomer functionality. During deposition, applied high powers can lead to an unexpected modifications in chemical structure and composition of the polymers due to monomer fragmentation such as opening of the aromatic chain and monomer oxidation, or even polymer oxidation. In this direction, nitrile group (C≡N) involves a loss of functionality due to the pyrrole group opening. It is worth to mention that, in the present study the absence of nitrile group (C≡N) band at 2200 cm^{-1} indicates the structural stability and functionality of PPy films grown at various glow powers. These results authenticate that the glow discharge plasma polymerization is one of the promising technique to produce quality PPy films by controlling the high fragmentation effect during the growth process. As evidenced from XRD studies, the presence of non-characteristic and broad headed peak at $2\theta = 23.5°$ (as shown in Figure 3) indicates the amorphous nature of the films.[43] Figure 4 Shows, AFM topography images of deposited PPy films as a function of glow discharge powers. The topography of the films prepared at lower Power value of 10 W, is observed to be uniform, denser, moderately smooth, and entire surface is composed of numerous irregular wrinkles of size about 100 nm [Figure 4(a)]. Considerable changes are observed in surface morphological features (such as grain size and shape, density of clusters, and surface roughness) with an increase of discharge powers to the higher values. For the PPy films grown at 50 W, the surface of the films is noticed to be composed of characteristic vertical cone shaped clusters of sizes in the range 400–500 nm [Figure 4(c)]. Roughness measurements are performed on several images taken from the same sample in order to estimate uniformity and homogeneity. The evaluated root mean square (rms) surface roughness of the grown films increased from 1.12 to 3.42 nm with the enhancement of DC power values from 10 to 50 W, respectively. This could be due to increase of number of islands consisting of aggregated polymers over ITO substrates and higher ratio value of "grain growth versus nuclei formation". In cold plasma polymerization process, ionization of pyrrole monomer is not so intense that layer growth overcomes the nuclei formation. With the enhancement of plasma powers, the rate of growth of formation of nucleation sites and their agglomeration over ITO substrate are relatively higher than layer growth process. Therefore, it is evident that DC glow discharge plasma polymerized PPy films have better uniformity and promising morphological characteristics.

The obtained results can be interpreted as follows: during the PPy film growth process in cold plasma polymerization technique, the activation of monomers and reactivation of the recombined molecules over surface of the substrates are essentially due to fragmentation by characteristic controlling parameter (W/FM) of established plasma in the plasma reactor.[33] This "W/FM" (W = power in J/s, F = monomer flow rate in mol/s and M = molecular weight of monomer in Kg/mol) is an apparent input energy per the unit of monomer molecule in J/Kg and magnitude of W/FM parameter is considered to be proportional to the concentration of activated species in the plasma region. Obviously for constant monomer flow rate (F) and molecular weight (M) values, the polymer formation rate (i.e.,

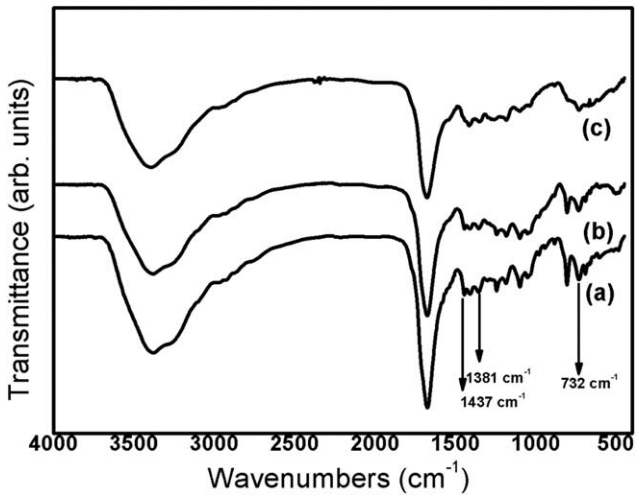

Figure 2. FTIR spectra of plasma polymerized PPy thin films deposited at different discharge power of (a) 10 W, (b) 30 W, and (c) 50 W.

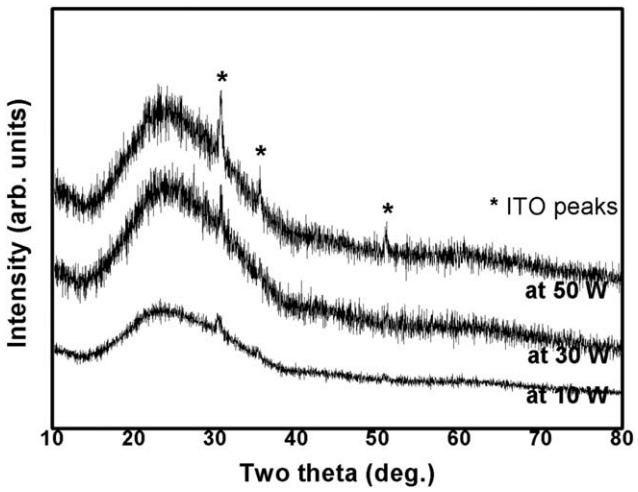

Figure 3. XRD spectra of PPy thin films deposited at different discharge powers.

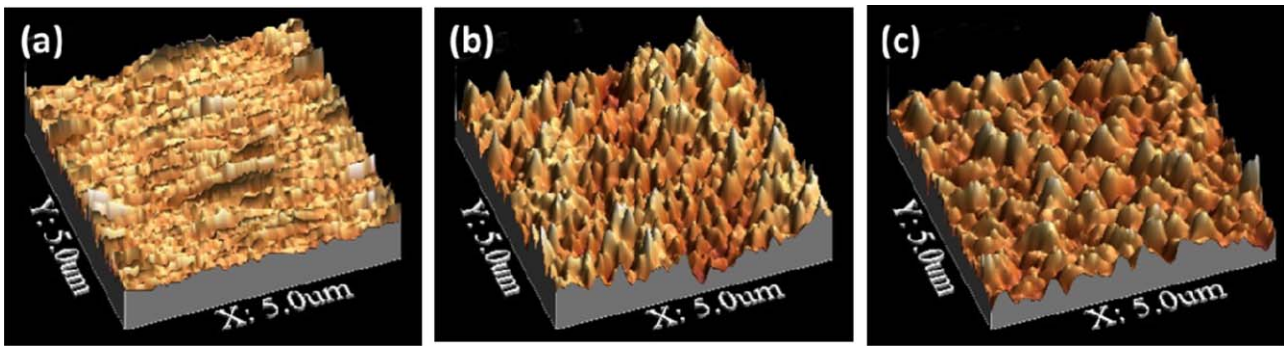

Figure 4. Atomic force micrographs of DC-discharge plasma polymerized PPy thin films prepared various discharge powers (a) 10 W, (b) 30 W, and (c) 50 W. [Color figure can be viewed in the online issue, which is available at wileyonlinelibrary.com.]

polymer deposition rate) is directly proportional to power of the established "plasma region" in the deposition chamber. Therefore, at lower deposition rates (i.e., at 10 W) less energetic activated monomer species reach the surface of substrates to form growth centers and later polymerize with each other to form uniform PPy thin films. Hence we can observe irregular wrinkles formation over surface of the substrates and generation of internal stresses in the matrix of polymer thin film during the growth as evidenced from Figure 4(a). The enhancement of plasma power to the higher values leads to the generation of higher concentration of activated species provided with higher energy. As a result, the as-deposited higher energetic active species can move over surface of the substrate toward active growth centers to agglomerate with each other in vertical direction to the substrate. This might be due to the enhancement of rate of mobility of active species than the rate of formation of growth centers over the surface of substrate provided with increase of micro voids inside the matrix of PPy thin films. This could be the reason for films grown at higher plasma power of 50 W were demonstrated distinguished surface morphology provided with higher root mean square (rms) roughness and composed of vertical spike shaped clusters. Interestingly, we could not observe considerable changes in structural properties in long range as a function of plasma power.

The characterization of optical studies of PPy films was performed by measuring the transmittance $T(\lambda)$, absorption $A(\lambda)$, and reflectance $R(\lambda)$ in the wavelength region 200–1200 nm. For many organic materials, the band to band transitions theory was applied to analyze the optical absorption at fundamental edge. Figure 5 shows, optical absorption spectra of PPy films prepared at various discharge powers. The Q–band present at $\lambda = 400$–600 nm is attributed to π–π^* transition from highest occupied molecular orbital (HOMO) to the lowest unoccupied molecular orbital (LUMO) in visible region.[44,45] The analysis of the absorption coefficient has been carried out to obtain the optical energy band gap (E_g), which is the most important parameter for organic and inorganic materials. The optical bandgap of the PPy films was estimated by applying Tauc's relationship.[46–48]

$$(\alpha h\vartheta)^n = A\left(h\vartheta - E_g\right) \quad (1)$$

In the above expression "α" represents absorption coefficient, A is a constant and $h\vartheta$ and E_g are incident photon energy and optical bandgap values, respectively. Here the index "n" is connected with the distribution of density of states and in the present study the n value is considered as 2 by representing the direct optical transition (i.e., $n = 2$). Figure 6 describes, the dependence of $(\alpha h\vartheta)^2$ on incident photon energy $h\vartheta$ and direct optical bandgap values for all films are determined from the intercept of the extrapolated linear part of the plot of $(\alpha h\vartheta)^2$ on the photon energy axis (abscissa).[49] Evidently, evaluated optical bandgap values are decreased as a function of discharge powers and PPy films prepared at lower discharge power of 10 W are exhibited higher band gap value of 2.72 eV. It is observed that, estimated bandgap values are decreased to the lower value of 2.53 eV with an increase of discharge power to the higher value of 50 W. The decrease in evaluated optical band gap values might be due to the modification of the structure of polymer matrix during the growth of thin films as a function of plasma power. In addition, during the plasma assisted polymerization process the rate of branching and cross linking of activated species on surface of substrates is directly proportional to the strength of plasma region in deposition chamber. As a result, the PPy films grown at lower plasma power of 10 W were not highly branched and cross linked to form three-dimensional networks. The increase of plasma power to the

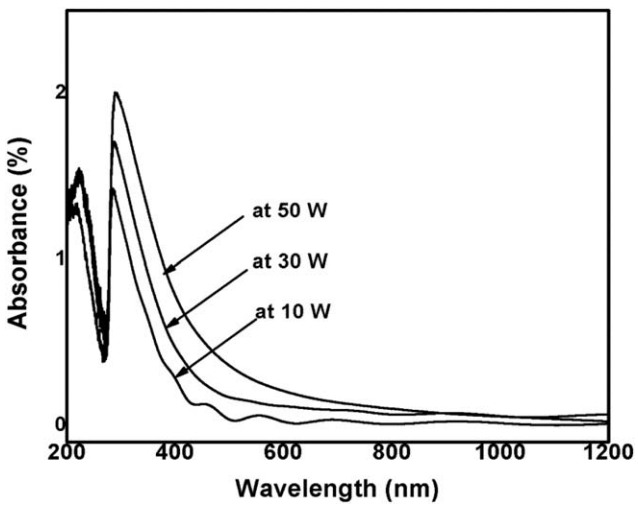

Figure 5. UV-VIS absorption spectra of PPy films synthesized at different discharge powers.

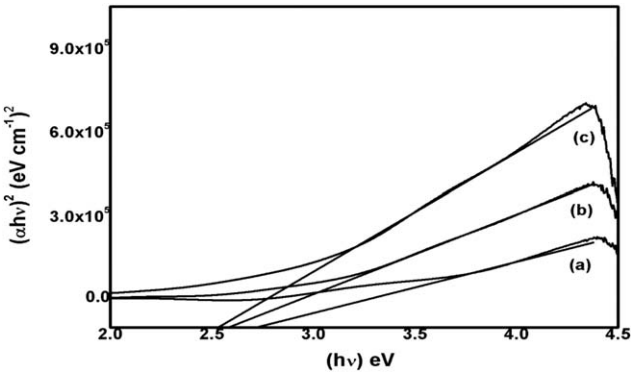

Figure 6. The $(\alpha h\upsilon)^2$ versus $(h\upsilon)$ graph and the optical energy gaps of the PPy films grown at various glow powers (a) 10 W, (b) 30 W, and (c) 50 W.

higher value of 50 W leads to enhancement of branching and cross linking of activated pyrrole monomer species and responsible for micro level modifications in structure of polymer matrix. The refractive indexes of grown films are estimated from the obtained reflection $R(\lambda)$ and estimated extinction data using the Fresnel formulae as follows[47,48]:

$$n = \left(\frac{1+R}{1-R}\right) + \left[\frac{4R}{(1-R)^2} - K^2\right]^{1/2} \quad (2)$$

where R is reflection coefficient, and $K = {}^{\alpha\lambda}/_{4\pi}$ is the extinction coefficient. Here α represents optical absorption coefficient, which can be evaluated by using the following expression.

$$\alpha = 2.303\left(\frac{A}{d}\right) \quad (3)$$

Where A, d are optical absorption and film thickness, respectively. Figure 7 illustrates the variation of refractive index as a function of wavelength for PPy films deposited at various discharge powers. Evidently, the estimated refractive indices of PPy films demonstrate oscillating behavior as a function of wavelength. This could be due to change in density of Polymer matrix and moderate thickness of the films as a function of discharge powers. Contact angle analysis offers an easy method for determining the wettability (or hydrophilicity) and adhesion of a given liquid on a solid surface. The study of surface wetting properties of polymers has a classical significance in the field of "Surface Engineering" and for potential applications such as lab-on-a-chip devices in micro fluids, self-cleaning properties and it became a synergy of micro/nano morphology and chemistry.[50,51] Wetting properties of freshly deposited PPy thin films studied using micro distilled water and by measuring contact angles for consecutive 50 frames and at a time interval of 5 s. The obtained results revealed that, estimated contact angles decline exponentially with respective to wetting time as shown in the Figure 8. Evidently after 250 s, PPy films grown at lower plasma power of 10 W were showed contact angle of 51.76° and observed to be decreased to 28.9° for the films grown at higher discharge power of 50 W. In comparison to all the films, the rate of decrease in contact angle values is noticed to be predominant for PPy films prepared at higher discharge powers and this could be due to enhancement of surface roughness of grown films as a function for plasma powers.[52] In the present investigation, as evidenced from AFM results, PPy films deposited at discharge power of 50 W are observed to be more hydrophilic. In the present study obtained results are closely matches with previously reported studies.[53,54]

Impedance spectroscopy (IS) is one of the promising analytical tools to analyze linear electrical response of materials of interest (including electrode effects) and the subsequent analysis of the response to yield useful information about physicochemical properties of the systems. In the present study, we recorded IS spectra for all PPy films at room temperature and investigated $Z^*(\omega)$ and $\varepsilon^*(\omega)$ parameters to understand electrical and dielectric properties as a function plasma power. Figure 9 shows the dependence of both real $Z^{|}$ and imaginary impedance $Z^{||}$ components of polymerized PPy films on applied frequency in the range 10 mHz–100 kHz. The $Z^{|}$ values are almost constant at lower and higher frequency regions, and interestingly decreased monotonically in intermediate frequency zone and [Figure 9(a)]. The peak maximum value of $Z^{||}$ is noticed to be shifted toward higher frequency region with the increase of plasma power [inset of Figure 9(a)]. The Nyquist plots for PPy films [Figure 9(b)]

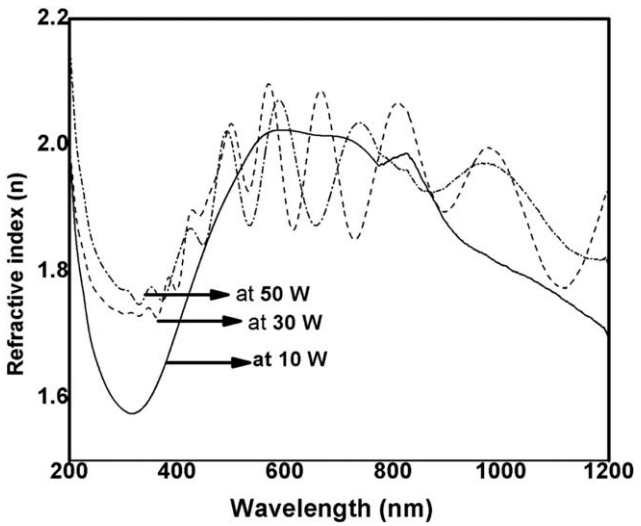

Figure 7. Spectral dependence of refractive index of PPy films grown at various discharge powers.

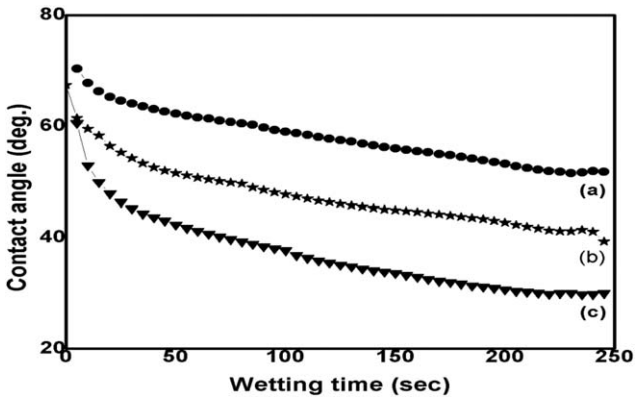

Figure 8. Surface wetting properties PPy films: (a) 10 W, (b) 30 W, and (c) 50 W.

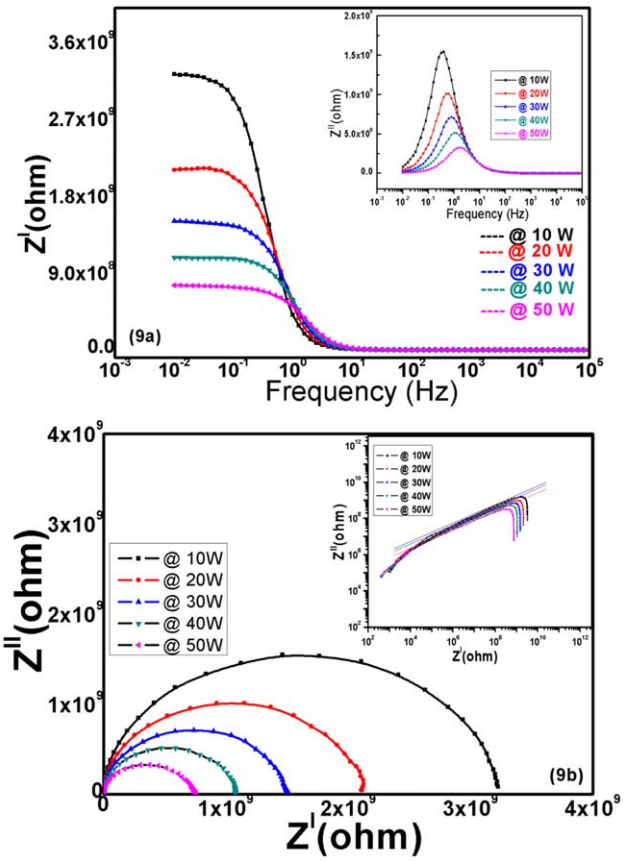

Figure 9. (a) Real and imaginary parts of impedance versus frequency for grown PPy films as a function of discharge powers. (b) Nyquist plots for PPy films at various conditions. [Color figure can be viewed in the online issue, which is available at wileyonlinelibrary.com.]

demonstrated characteristic single semicircles close to origin, which is a typical for single layered thin films.[55] These semicircles divulge the presence of the parallel combination of bulk resistance corresponding to migration of ions and bulk capacitance (due to the immobile polymer chains). Therefore, the frequency response for the grown thin films can be represented by an equivalent electrical circuit consisting of series resistance (R_s) corresponding to contact resistance of the ITO/polymer interface and the bulk resistance (R_p) in the parallel RC network, bulk capacitance (C_p) associated to layer resistance of the anthracene derivative, geometric capacitance of the polymer layer, respectively. The estimated slope values from Nyquist plots on log–log scale are observed to be nearly equal to 0.5 [inset of Figure 9(b)] and it signifies the single characteristic relaxation time.[56] From the Nyquist plots bulk resistance (R_b) was estimated from the intercept of the plot with the real impedance axis. The conductivity can be calculated from the following equation[57] and tabulated in Table I. The estimated conductivity values are observed to be increased with an increase in glow power.

$$\sigma_{dc} = \left(\frac{I}{R_b}\right) X \left(\frac{t}{A}\right) \tag{4}$$

Where t is film's thickness, R_b is the bulk resistance of the sample, and A is the effective area.

Dielectric measurements have been carried out by sandwiching the PPy films between two ITO electrodes and by employing EG&G 273A galvanostat-potentiostat/impedentiometer controlled by the impedance software M398 in order to acquire the real and imaginary part of resultant impedance. Experimentally, real and the imaginary parts of dielectric constant have been calculated from impedenziometric data by using following equations:

$$\varepsilon^{|} = -\frac{X}{(X^2+R^2)}\frac{d}{\varepsilon_0 A}\frac{1}{2\pi f} \tag{5}$$

$$\varepsilon^{||} = \frac{R}{(X^2+R^2)}\frac{d}{\varepsilon_0 A}\frac{1}{2\pi f} \tag{6}$$

In the above expressions, R, X, d, A, and f represent real impedance, Reactance, thickness of the sample, area of cell surface, and frequency of applied electric field, respectively. The resultant modulus of the complex dielectric constant is evaluated as follows.

$$\varepsilon^* = \sqrt{(\varepsilon^{|})^2 + (\varepsilon^{||})^2} \tag{7}$$

In order to interpret the influence of plasma power on measured dielectric relaxation of grown PPy films, $\varepsilon^*(f)$ can be described by Havriliak-Nagami function (which is an empirical modification of the Debye relaxation model, accounting for the asymmetry and broadness of the dielectric dispersion curve) with the addition of a conductivity contribution (last term) present at lower frequencies.

$$\varepsilon^*(f) = \varepsilon_\infty + \sum_{j=1} \frac{\Delta\varepsilon}{[1+i(2\pi f)/(2\pi f_j)^{\alpha}]^{\beta}} - \frac{i\sigma}{\varepsilon_{0(\omega)^{\xi}}} \tag{8}$$

Here, $\Delta\varepsilon = (\varepsilon_S - \varepsilon_\infty)$ indicates dielectric strength, ε_S and ε_∞ are permittivity values at lower and higher frequencies, respectively. f_j is the corresponding relaxation frequency of the medium, "α" and "β" describe the asymmetry and broadness of

Table I. Fitting Parameters for PPy Films Deposited at Various Discharge Powers

Plasma power (W)	Δε (V/M)	ω	α	β	σ_{fit} (S/m) × 10^{-12}	σ_{est} (S/m) × 10^{-12}	ξ
10	0.12	0.001	0.87	0.5	1.35	1.37	0.96
20	0.14	0.005	0.82	0.79	2.11	2.00	0.99
30	0.2	0.009	0.79	0.99	2.97	2.92	0.97
40	0.3	0.009	0.90	0.99	3.97	4.08	0.96
50	0.7	0.01	0.99	0.99	6.00	5.82	0.99

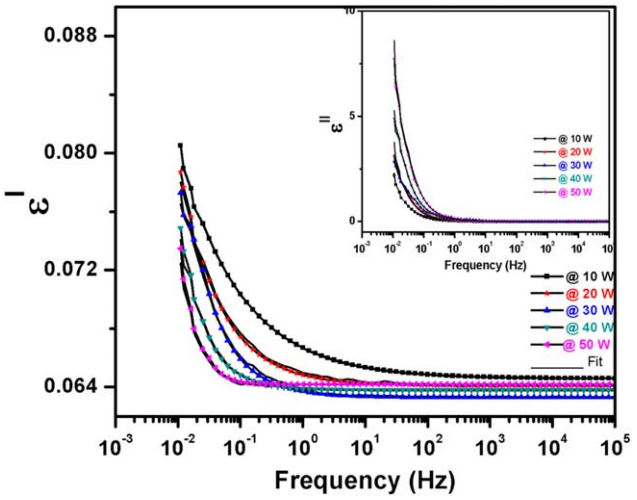

Figure 10. Behavior of estimated dielectric constants of grown films as a function of frequency (solid black line represents the fit). [Color figure can be viewed in the online issue, which is available at wileyonlinelibrary.com.]

the corresponding spectra. "σ" is related to conductivity, and "ξ" is a fitting parameter responsible for the slope of the conductivity.[58,59]

Figure 10 illustrates the variation of characteristic $\varepsilon^{|}(f)$ and $\varepsilon^{||}(f)$ values as a function of applied frequency. At lower frequency region, the $\varepsilon^{|}(f)$ values are increased with decrease in applied frequency and this similar behavior is observed for many polymers, it could be due to contribution of free charge carriers conduction in the matrix of PPy thin films.[60] At higher frequency region, $\varepsilon^{|}(f)$ values are independent of applied frequency. Because at high frequency regions, the free charge carriers diffusion along direction of the applied electric field becomes zero due to rapid periodic reversal of the applied electric field. Estimated dielectric constant values of PPy films are decreased with an increase of discharge power. The dielectric loss $\varepsilon^{||}(f)$ values of grown PPy films decreased exponentially at lower frequency region and became independent of frequency at higher frequency region as shown in inset of Figure 10. The dielectric strength "Δε" provides the information about relaxation strength of polymer matrix and estimated Δϵ values increased slightly with increase of plasma power. At lower plasma power values, the interlinking of activated polymer spices show a preferential dipolar orientation in the direction of its polarization. With the increase of plasma power, the activated polymer species oppose to show a preferential dipolar orientation in the direction of polarization and this leads to slight increase in dielectric strength values. The Cole–Cole plots for grown PPy films are fitted by Mathematica curve fitting tool (as shown in Figure 11)[61] and obtained respective dielectric strength, conductivity values are provided in Table I. Estimated and fitted conductivity results are in congruent with each other and noticed to be increased appreciably from 1.35×10^{-12} S/m to 6.0×10^{-12} S/m with an increase of plasma powers from 10

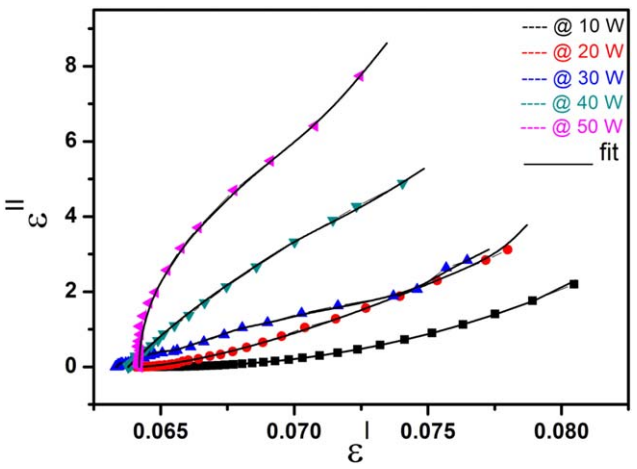

Figure 11. Cole–Cole plots for DC glow discharge plasma polymerized PPy films. [Color figure can be viewed in the online issue, which is available at wileyonlinelibrary.com.]

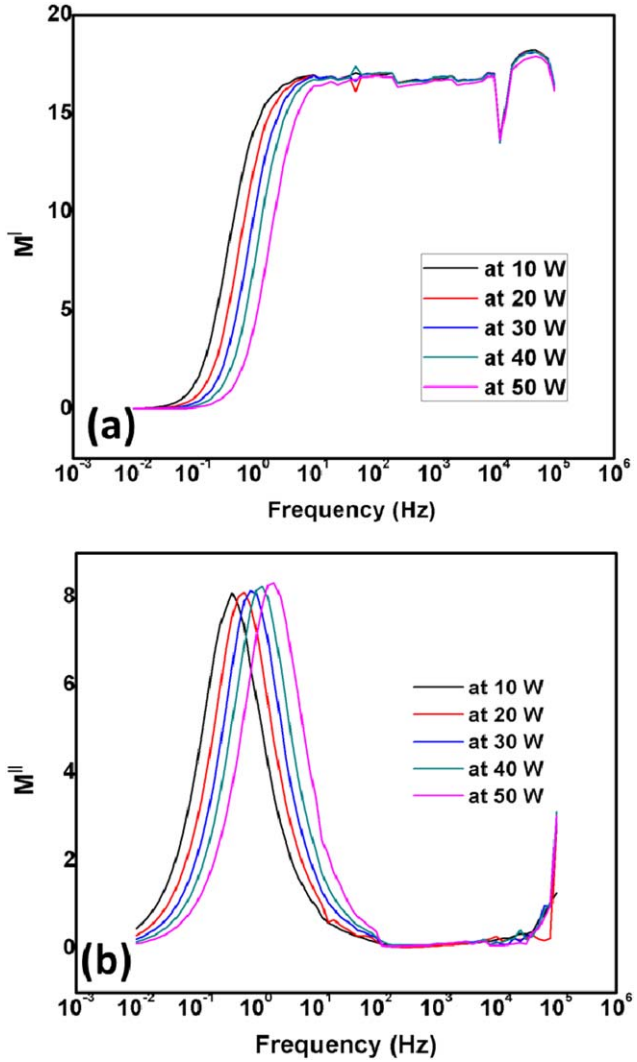

Figure 12. (a) Real and (b) imaginary parts of electric modulus versus frequency for the PPy films at various discharge powers. [Color figure can be viewed in the online issue, which is available at wileyonlinelibrary.com.]

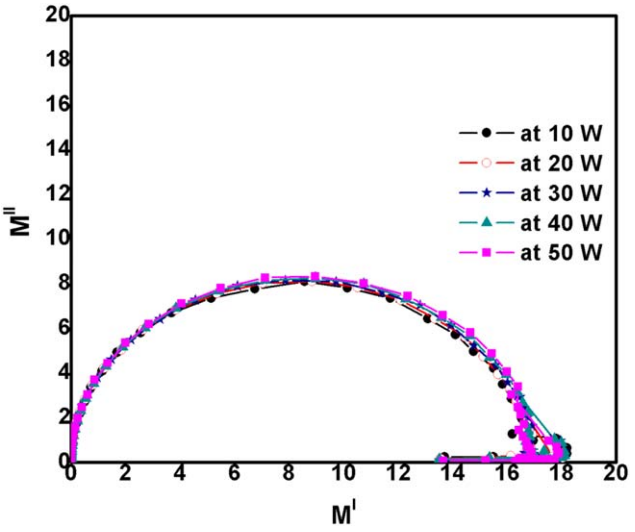

Figure 13. Argand plots for PPy films prepared at different discharge powers. [Color figure can be viewed in the online issue, which is available at wileyonlinelibrary.com.]

W to 50 W, respectively. It reveals the increase of migration of immobile species or defects in the polymer material as a function plasma power.

Complex modulus analysis is an alternative approach to explore electrical properties of the material and to magnify any other effects present in the sample as a result of different relaxation time constants. It is an important and convenient tool to determine, analyze and interpret the dynamical aspects of electrical transport phenomena (i.e., parameters such as charge carrier hopping rate, conductivity relaxation time, etc.). A complex electric modulus has been used to investigate the conductivity relaxation phenomena, because it suppresses the effects of electrode polarization (EP) to give a clear picture of electrical properties. Complex electric modulus can be estimated from the impedance data using following expression.[62]

$$M^* = M^{|}(\omega) + jM^{||}(\omega). \quad (9)$$

$$M^{|} = \omega C_0 Z_i. \quad (10)$$

$$M^{||} = \omega C_0 Z_r. \quad (11)$$

Here $M^{|}$, $M^{||}$ and Z_i, Z_r represent real and imaginary parts of the electric modulus and impedances, respectively. The complex dielectric function, ε^*, which consists of dielectric constant and loss in materials property depends on frequency, temperature, and structure. At low frequency both of them ($\varepsilon^{|}$ and $\varepsilon^{||}$) are very high due to EP effect.[63] To reduce the effect of EP, Macedo and coworkers have established the electric modulus formalism.[64] The frequency dependence of $M^{|}$ for PPy films grown at various discharge powers is shown in Figure 12(a). It is obvious that $M^{|}$ reaches a maximum saturation at high frequency and this type behavior is an indicative of negligible EP phenomenon in the test material. The plots of $M^{||}$ versus frequency [as shown in Figure 12(b)] exhibit peaks for $M^{||}$ at different frequencies corresponding to the different discharge powers. The peak maxima is observed to shift towards higher frequency side with an increase of discharge powers. The respective Argand plots for PPy films demonstrated complete semicircular shape (as shown in Figure 13) and the respective diameter of the semicircles are found to be independent of discharge powers.

CONCLUSIONS

We have synthesized Polypyrrole thin films by DC glow discharge plasma polymerization technique and investigated the influence of discharge power on microstructural and dielectric properties. As evidenced from XRD measurements PPy films prepared at various discharge powers are observed to be amorphous in nature. The presence of characteristic peaks in FTIR spectra reveals that DC-glow discharge plasma polymerization is a promising technique to produce structurally less defective PPy films by controlling high fragmentation effect during the growth process. In the present study, as a function of discharge power, we observed significant modifications in surface morphology, optical, and dielectric properties grown PPy films. For films prepared at higher discharge power of 50 W, the surface morphology of the films is observed to be composed of vertical spike shaped clusters with an estimated rms surface roughness of 3.42 nm. The absorption band in UV-Vis region is interpreted in terms of π–π^* excitation and evaluated optical band gap values are noticed to be decreased to 2.53 eV with an increase of discharge power to the higher value of 50 W. In the present work, significantly the hydrophilicity of Polypyrrole films increases with increase in discharge powers. The dielectric strength and conductivity of grown films are increased appreciably as a function of discharge power and found to be 0.7 V/m and 6×10^{-12} s/cm for films prepared at discharge power of 50 W.

ACKNOWLEDGMENTS

Work supported by the research project "Proof of Concept Network" (PoCN), "Nanocompositi basati su materiali morbidi (soft matter) ottenuti mediante la polimerizzazione al plasma freddo" – UniCAL 08 - Consorzio per l'Area di ricerca scientifica e tecnologica di Trieste. The authors acknowledge the INERA EU project Research Potential "Research and Innovation Capacity Strengthening of ISSP-BAS in Multifunctional Nanostructures" (FP7 REGPOT-2012-2013-1).

REFERENCES

1. Christopher, J. T.; Michael, A. B.; Neil, D. T.; Edward, J. K.; Michael, L. C. *Nano Lett.* **2014**, *14*, 3096.
2. Sukyoung, H.; Hosung, S.; Dong-Cheol, J.; Long, W.; Jeon, G. H.; Changsik, S.; Yunseok, K. *Sci. Rep.* **2015**, DOI: 10.1038/srep11201.
3. Alzari, V.; Sanna, V.; Biccai, S.; Caruso, T.; Politano, A.; Scaramuzza, N.; Sechi, M.; Nuvoli, D.; Sanna, R.; Mariani, A. *Compos. B* **2014**, *60*, 29.
4. Jianguo, M.; Ying, D.; Anthony, L. A.; Lei, F.; Zhenan, B. *J. Am. Chem. Soc.* **2013**, *135*, 6724.
5. Markus, G.; David, C. M.; Heinz-Georg, N.; Ulrich, S.; Dieter, N.; Christoph, B.; Klaus, M. *Nature* **2000**, *405*, 661.

6. Franciele, W.; Deepak, P. D.; Marcio, V.; Rudolf, H.; Pedro, G.-R. *J. Solid State Electrochem.* **2015**, DOI: 10.1007/s10008-015-2960-2.
7. Jianhang, H.; Zhanhong, Y.; Bin, Y.; Ruijuan, W.; Tingting, W. *J. Power Sources* **2014**, *271*, 143.
8. Valeria, A.; Daniele, N.; Vanna, S.; Tommaso, C.; Salvatore, M.; Nicola, S. *AIP Adv.* **2016**, DOI: 10.1063/1.4943672.
9. Yang, J.; Cho, M.; Pang, C.; Lee, Y. *Sens. Actuators B Chem.* **2015**, *211*, 93.
10. Merisalu, M.; Kahro, T.; Kozlova, J.; Niilisk, A.; Nikolajev, A.; Marandi, M.; Floren, A.; Alles, H.; Sammelselg, V. *Synth. Met.* **2015**, *200*, 16.
11. Wang, K.; Zhang, X.; Li, C.; Zhang, H.; Sun, X.; Xu, N.; Ma, Y. *J. Mater. Chem.* **2014**, *2*, 19726.
12. Rodriguez, J.; Grande, H. J.; Otero, T. F. In Handbook of Organic Conductive Molecules and Polymers; Nalwa, H. S., ed.; Wiley: New York, **1997**; p 415.
13. Scrosati, B. Applications of Electroactive Polymers; Chapman & Hall: London, **1993**.
14. Sadki, S.; Schottland, P.; Brodie, N.; Sabouraud, G. *Chem. Soc. Rev.* **2000**, *29*, 283.
15. Xiong, W.; Hu, X.; Wu, X.; Zeng, Y.; Wang, B.; He, G.; Zhu, Z. *J. Mater. Chem. A* **2015**, *3*, 17209.
16. Yang, C.; Shen, J.; Wang, C.; Fei, H.; Bao, H.; Wang, G. *J. Mater. Chem. A* **2014**, *2*, 1458.
17. Huang, S.; Chen, P.; Lin, W.; Lyu, S.; Chen, G.; Yin, X.; Chen, W. *RSC Adv.* **2016**, *6*, 13359.
18. Janata, J.; Josowicz, M. *Nat. Mater.* **2003**, *2*, 19.
19. Lu, S.; Zhang, X.; Feng, T.; Han, R.; Liu, D.; He, T. *J. Power Sources* **2015**, *274*, 1076.
20. Xia, J.; Chena, L.; Yanagida, S. *J. Mater. Chem.* **2011**, *21*, 4644.
21. Zhang, X.; Zhang, J.; Song, W.; Liu, Z. *J. Phys. Chem. B* **2006**, *110*, 1158.
22. Wojcik, K.; Grzeszczuk, M. *J. Solid State Electrochem.* **2015**, *19*, 1293.
23. Mehrnoosh, M.; Behzad, P.; Shams, M. *Thin Solid Films* **2015**, *583*, 255.
24. Aviraj, A. J.; Jyotiprakash, B. Y.; Sandip, V. K.; Vaishali, S. P.; Mahadik, D. B.; Harish, C. B.; Vijaya, P.; Puri, R. K. *J. Phys. Chem. Solids* **2015**, *80*, 78.
25. Franciele, W.; Deepak, P. D.; Marcio, V.; Rudolf, H.; Pedro, G.-R. *J. Solid State Electrochem.* **2016**, *20*, 901.
26. Jayamurugan, P.; Ponnuswamy, V.; Subba Rao, Y. V.; Ashokan, S.; Meenakshisundar, S. *Mater. Sci. Semicond. Process.* **2015**, *39*, 205.
27. Farnaz, T.; Naader, A. *J. Electroanal. Chem.* **2015**, *746*, 39.
28. Karaman, M.; Uçara, T. *Appl. Surf. Sci.* **2016**, *362*, 210.
29. Gürsoy, M.; Karaman, M. *Chem. Eng. J.* **2016**, *284*, 343.
30. Teslaru, T.; Topala, I.; Dobromir, M.; Pohoata, V.; Curecheriu, L.; Dumitrascu, N. N. *Mater. Chem. Phys.* **2016**, *169*, 120.
31. Jeong, D.-C.; Wen, L.; Kim, S.; Nam, J.-D.; Han, J. G.; Song, C. *Surf. Coat. Technol.* **2014**, *259*, 27.
32. Yasuda, H.; Hirotsu, T. *J. Polym. Sci. Polym. Chem. Ed.* **1978**, *16*, 743.
33. Nastase, F.; Mihaiescu, D.; Nastasea, C.; Mireac, C.; Burzob, I.; Ioan, S. *Compos. A* **2005**, *36*, 503.
34. Kojima, T.; Takaku, H.; Urata, Y.; Gotoh, K. *J. Appl. Polym. Sci.* **1993**, *48*, 1395.
35. Zhang, J.; Wu, M. Z.; Pu, T. S.; Zhang, Y. Z.; Jin, R. P.; Tong, Z. S. *Thin Solid Films* **1997**, *307*, 14.
36. Fally, F.; Doneux, C.; Riga, J.; Verbist, J. J. *J. Appl. Polym. Sci.* **1995**, *56*, 597.
37. Zhang, C.; Hu, J.; Cong, J.; Zhao, Y.; Shen, W.; Toyoda, H.; Nagatsu, M.; Meng, Y. *J. Power Sources* **2011**, *196*, 5386.
38. Hakansson, E.; Lin, T.; Wang, H.; Kaynak, A. *Synth. Met.* **2006**, *156*, 1194.
39. Dhillon, A.; Kaur, A.; Srivastava, A. K.; Avasthi, D. K. *Prog. Org. Coat.* **2010**, *69*, 396.
40. Wiliams, D. H.; Fleming, I. Spectroscopic methods in organic chemistry, 5th ed.; Tata McGraw-Hill: New Delhi, **2004**.
41. Singh, R.; Narula, A. K.; Tandon, R. P.; Rao, S. U. M.; Panwar, V. S.; Mansingh, A.; Chandra, S. *Synth. Met.* **1996**, *79*, 1.
42. Wang, J.; Neoh, K. G.; Kang, E. T. *Thin Solid Films* **2004**, *446*, 205.
43. Ouyang, J. Y.; Li, Y. F. *Polymer* **1997**, *38*, 3997.
44. El-Nahass, M. M.; Ammar, A. H.; Atta, A. A.; Farag, A. A. M.; El-Zaidia, E. F. M. *Opt. Commun.* **2011**, *284*, 2259.
45. Kandaz, M.; Güney, O.; Senkal, F. B. *Polyhedron* **2009**, *28*, 3110.
46. Omed, G. A.; Shujahadeen, B. A.; Khalid, M. O.; Yousif, M. S. *J. Mater. Sci.: Mater. Electron.* **2015**, *26*, 5303.
47. Shujahadeen, B. A.; Hameed, M. A.; Ahang, M. H.; Awder, B. F.; Rawaz, M. W.; Rekawt, T. H. *J. Mater. Sci.: Mater. Electron.* **2015**, *26*, 8022.
48. Cruz, G. J.; Morales, J.; Olayo, R. *Thin Solid Films* **1999**, *342*, 119.
49. Ashery, A.; Farag, A. A. M.; Shenashen, M. A. *Synth. Met.* **2012**, *162*, 1357.
50. Barberoglou, M.; Zorba, V.; Pagozidis, A.; Fotakis, C.; Stratakis, E. *Langmuir* **2010**, *26*, 13007.
51. Gupta, N. D.; Das, S.; Das, N. S.; Banerjee, D.; Sarkar, D.; Chattopadhyay, K. K. *J. Appl. Polym. Sci.* **2014**, *131*, DOI: 10.1002/app.39771.
52. Wenzel, R. N. *Ind. Eng. Chem.* **1936**, *28*, 988.
53. Thombare, J. V.; Lohar, G. M.; Shinde, S. K.; Dhasade, S. S.; Rath, M. C.; Fulari, V. J. *Electron. Mater. Lett.* **2015**, *11*, 266.
54. Jonda, C.; Andrea, B. R. M. *Chem. Mater.* **1999**, *11*, 2429.
55. Seong, H. K.; Kang-Hoon, C.; Hyang-Mok, L.; Do-Hoon, H.; Lee-Mi, D.; Hye Yong, C.; Taehyoung, Z. *J. Appl. Phys.* **2000**, *87*, 882.
56. Kiran Kumar, K.; Ravi, M.; Pavani, Y.; Bhavani, S.; Sharma, A. K.; NarasimhaRao, V. V. R. *J. Membr. Sci.* **2014**, *454*, 200.
57. Zang, J.; Li, C. M.; Bao, S.-J.; Cui, X.; Bao, Q.; Sun, C. Q. *Macromolecules* **2008**, *41*, 7053.

58. Havriliak, S.; Negami, S. *Polymer* **1967**, *8*, 161.

59. Marino, L.; Marino, S.; Wang, D.; Bruno, E.; Scaramuzza, N. *Soft Matter* **2014**, *10*, 3842.

60. Pillai, P. K. C.; Khurana, P.; Tripathi, A. *J. Mater. Sci. Lett.* **1986**, *5*, 629.

61. Marino, L.; Ionescu, A. T.; Daniela, P.; Marino, S.; Bruno, E.; Scaramuzza, N. *J. Appl. Phys.* **2014**, *116*, 114101.

62. Migahed, M. D.; Ishra, M.; Fahmy, T.; Barakat, A. *J. Phys. Chem. Solids* **2004**, *65*, 1121.

63. Okutan, M.; Sentürk, E. *J. Non-Cryst. Solids* **2008**, *354*, 1526.

64. Agrawal, S. L.; Singh, M.; Asthana, N.; Dwivedi, M. M.; Pandey, K. *Int. J. Polym. Mater.* **2011**, *60*, 276.